

# High-fidelity spatially resolved multiphoton counting for quantum imaging applications

Radosław Chrapkiewicz,<sup>1,\*</sup> Wojciech Wasilewski,<sup>1</sup> and Konrad Banaszek<sup>1</sup>

<sup>1</sup>*Faculty of Physics, University of Warsaw, ul. Hoża 69, Warsaw, Poland*

*\*Corresponding author: radekch@fuw.edu.pl*

Compiled May 20, 2014

We present a method for spatially resolved multiphoton counting based on an intensified camera with the retrieval of multimode photon statistics fully accounting for non-linearities in the detection process. The scheme relies on one-time quantum tomographic calibration of the detector. Faithful, high-fidelity reconstruction of single- and two-mode statistics of multiphoton states is demonstrated for coherent states and their statistical mixtures. The results consistently exhibit classical values of Mandel and Fano parameters in contrast to raw statistics of camera photo-events. Detector operation is reliable for illumination levels up to the average of one photon per an event area, substantially higher than in previous approaches to characterize quantum statistical properties of light with spatial resolution. © 2014 Optical Society of America

OCIS codes: (030.5260) Photon counting; (270.5570) Quantum detectors; (270.5290) Photon statistics.

Spatial degree of freedom of light is a vital and applicable resource to realize many quantum protocols [1, 2]. In parallel, photon number resolved detection becomes increasingly important in quantum protocols [3–5]. In both cases dedicated diagnostic techniques need to be developed. So far, multiphoton states of light have been investigated with the use of photon number resolving (PNR) detectors such as loop detectors [6, 7], multipixel photon counters [8] or transition-edge sensors [9]. In parallel recent advances in camera systems enabled experiments in entanglement imaging [10, 11], ghost imaging [12] and sub-shot noise imaging [13]. Single photon sensitive cameras such as intensified CCD (ICCD) and electron multiplied CCD (EM CCD) have been also utilized as PNR detectors however their use was severely limited to low illumination levels imposing trade-off between high-spatial resolution or PNR capability [10, 14–17].

In this Letter, we introduce and demonstrate experimentally a versatile method to measure quantum statistical properties of optical radiation with spatial and photon number resolution. The method utilizes a single photon sensitive camera whose pixels are grouped at the post-processing stage into tiles – “macropixels” that provide photon number resolving capability. Individual tiles are calibrated using techniques developed for quantum detector tomography [18, 19] which fully take into account the non-linear response of the camera, including saturation effects. Our approach extends the operation of the detector to substantially higher illumination levels than could be handled in previous experiments [10, 14–17]. In most of these works, the raw statistics of camera photo-events was directly identified with the input photon number distribution. Such an assumption misinterprets cases when two or more photons generate a single photo-event, leading to artificial non-classical effects in photon statistics [20] when the detector is illuminated with classical light. Moreover, joint measurements at multiple spatial locations can yield sub-

Poissonian correlations for such classical input states. As a result, unambiguous verification of non-classical features of detected radiation becomes difficult if not impossible. Our method avoids these issues altogether by tomographic calibration of the detection process in a single experimental run and appropriate raw data processing. Characteristics of the detector such as the effective spatial resolution and the accessible photon number range can be defined at the postprocessing stage.

Our experimental setup, depicted in Fig. 1(a) is based on an intensified sCMOS (I-sCMOS) camera which operates similarly to conventional ICCD cameras. Incident photons induce photoelectron emission at the photocathode of the image intensifier. Each generated photoelec-

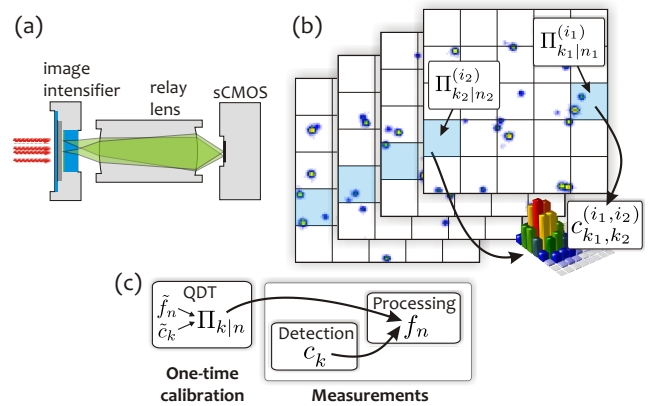


Figure 1. (a) Schematic of the detection on intensified sCMOS camera. (b) Camera detection area with photo-events bright spots is arbitrarily divided on tiles array in postprocessing stage. (c) Operation procedure initialized by one-time tomographic calibration yields conditional probabilities  $\Pi_{k|n}$  for each tile.  $\Pi_{k|n}$  allow to reconstruct initial photon number distributions  $f_n$  from raw photo-events statistics  $c_k$  in subsequent measurement runs.

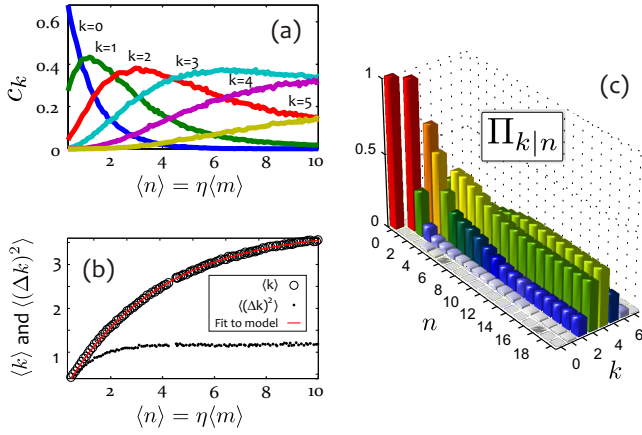


Figure 2. Exemplary operation of a single tile. (a) Photo-events statistics  $c_k$  measured with coherent state illumination versus mean number of photons  $\langle n \rangle = \eta \langle m \rangle$ . (b) Mean  $\langle k \rangle$  and variance  $\langle (\Delta k)^2 \rangle$  of photo-events. Fit to the model Eq. (3) yielded  $N = 3.8$ . (c) Quantum detector tomography [18, 19] resulted in conditional probability values  $\Pi_{k|n}$  fully determining the tile operation.

tron initiates a macroscopic avalanche in a micro-channel plate, subsequently converted into an intense localized flash on the phosphor screen. Flashes are registered as 5-pixel full width at half maximum spots on a sCMOS sensor. A typical image on the sensor is shown Fig. 1(b). The average intensity of the brightest pixel is approx. 500 times higher than the camera noise level. A spot is identified in real time by software as an individual photo-event via its central pixel which has to be brighter than all its neighbors up to a three pixel radius, and to exceed the noise level at least five times. The precise location of the spot is found by fitting a two dimensional paraboloid to the logarithm of the pixel intensity within the same three pixel radius.

The spatial resolution of the detection system is defined at the postprocessing stage by dividing the acquisition region into tiles, as exemplified in Fig. 1(b). Each tile, labeled with an index  $i$ , will be treated as a PNR quantum detector described by a conditional probability distribution  $\Pi_{k|n}^{(i)}$  which relates the number  $k$  of registered photo-events to the number  $n$  of incident photons that generated photoelectrons. For a single tile, the photo-event statistics  $c_k^{(i)}$  depends on the photon number distribution  $f_n^{(i)}$  through a standard expression

$$c_k^{(i)} = \sum_n \Pi_{k|n}^{(i)} f_n^{(i)}. \quad (1)$$

This formula can be readily generalized to multiple tiles, which e.g. for a pair of tiles  $(i_1, i_2)$  takes the form

$$c_{k_1, k_2}^{(i_1, i_2)} = \sum_{n_1, n_2} \Pi_{k_1|n_1}^{(i_1)} \Pi_{k_2|n_2}^{(i_2)} f_{n_1, n_2}^{(i_1, i_2)}. \quad (2)$$

where  $c_{k_1, k_2}^{(i_1, i_2)}$  and  $f_{n_1, n_2}^{(i_1, i_2)}$  are respectively the joint photo-

event statistics and the joint photon number distribution. If the input state of light is known, the relation given by Eq. (1) can be applied to find the conditional probabilities  $\Pi_{k|n}^{(i)}$  using the general methods of quantum detector tomography (QDT) [18, 19]. Resorting to QDT-based calibration fully takes into account the specifics of the camera operation and extends the ability of the setup to resolve higher photon numbers. Once the coefficients  $\Pi_{k|n}^{(i)}$  are found in a one-time procedure, Eqs. (1), (2) and their multidimensional generalizations can be used to reconstruct spatially resolved photon number distributions from joint photo-event statistics. The operation procedure is summarized in Fig. 1(c).

In order to perform QDT we used as probe states 100 ns–10  $\mu$ s laser pulses excised from an acousto-optical modulator from a continuous wave laser beam operating at a wavelength 795 nm. The quantum efficiency of the photocathode at this wavelength was measured to be  $\eta = 20\%$ . The laser beam was attenuated by a set of calibrated neutral density (ND) filters and its power was monitored on calibrated photodiode along all measurements. The beam was shaped into circular flat-top profile uniformly illuminating the acquisition region. Post-selected parts of the region served as model tiles. For an individual tile we measured the photo-event statistics  $c_k$ , its mean  $\langle k \rangle$  and variance  $\langle (\Delta k)^2 \rangle$  for different mean number of incoming photons  $\langle m \rangle$  as presented in Fig. 2 (a-b). The plots are parametrized with the number of incoming photons  $\langle m \rangle$  related to the number of generated photoelectrons  $\langle n \rangle = \eta \langle m \rangle$ . Each data point was obtained from acquisition of  $10^4$  frames.

We found that the mean number of photo-events  $\langle k \rangle$  fits to the model of  $N$  on-off detectors with QE =  $\eta$  uniformly illuminated by coherent state [21]:

$$\langle k \rangle = N(1 - e^{-\eta \langle m \rangle / N}). \quad (3)$$

Here the fit parameter  $N$  plays a role of the equivalent number of on-off detectors related to the single photo-event spots areas.  $N$  is proportional to the tile size which in our system is approximately  $N \times 25$  sCMOS pixels. Because the absolute measurement of a mean photon number  $\langle m \rangle$  using calibrated ND filters and the photodiode could be realized only for the entire laser beam, we repeated fits to Eq. (3) to determine precisely the fraction of light incident of a specific tile.

The measured photo-event statistics  $c_k$  (Fig. 2(b)) and the Poissonian statistics  $f_n$  of the probe states were used to find the conditional probabilities  $\Pi_{k|n}$  of the single tile in QDT by numerical convex optimization algorithm [18, 19]. The result of QDT is depicted in Fig. 2 (c). It is seen that a tile of the intensified camera saturates in a different manner than typical multiplexed detector. For large  $n' > n_{\text{sat}}$  the tile returns a stochastic number of photo-events  $k$  given by probability distribution  $\Pi_{k|n'} = \Pi_{k|n_{\text{sat}}}$ . This also implies that the variance of the number of photo-event counts  $\langle (\Delta k)^2 \rangle$  converges to the nonzero value as we observed in Fig. 2(a).

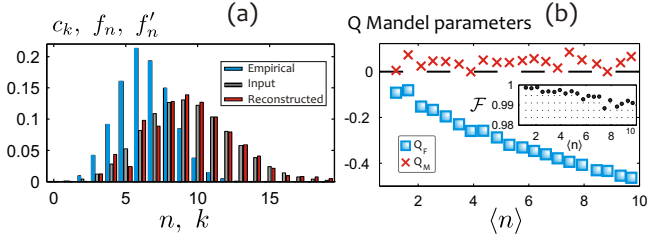


Figure 3. (a) Exemplary reconstruction of photo-event statistics  $f'_n$  based on measured counts statistics  $c_k$  at tile of size  $N = 12$ . Mean number of photons  $\langle n \rangle = 9.3$ , mean number of photo-events  $\langle k \rangle = 6.5$ . (b) Mandel parameters for photo-events  $Q_F$ , for reconstructed statistics  $Q_M$  for coherent states with variable mean photon number  $\langle n \rangle$ . In the box fidelity of reconstruction.

We used the conditional probabilities  $\Pi_{k|n}$  to reconstruct statistics of the known, test states to validate and quantify the effectiveness of our method. The reconstruction process relies on convex optimization algorithms analogously to QDT [18, 19] with  $f_n$  as the unknowns to be determined. As test states we employed coherent states available at hand and their statistical mixtures.

For one mode statistics we evaluate Mandel parameter  $Q_M = \langle (\Delta n)^2 \rangle / \langle n \rangle - 1$  while for two mode, joint statistics we evaluate the Fano noise reduction factor:  $R = \langle (\Delta(n_1 - n_2))^2 \rangle / (\langle n_1 \rangle + \langle n_2 \rangle)$ . For classical states we always have  $Q_M \geq 0$  and  $R \geq 1$ . Because the test states lay on the boundary between classical and non-classical states, they provide a sensitive probe into saturation effects. As a qualitative measure of the effectiveness of our method, we evaluated the fidelity  $\mathcal{F}$  between the input and the reconstructed statistics.

At first we performed state reconstruction for one mode coherent state illuminating the tile of the size determined by equivalent number of on-off detectors equals  $N = 12$  found from Eq. (3). In Fig. 3 (a) we compare measured empirical photo-event distribution  $c_k$  with *a priori* known input statistics  $f_n$  and reconstructed statistics  $f'_n$ . Here the Mandel parameter evaluated directly for the measured photo-event statistics  $Q_F = \langle (\Delta k)^2 \rangle / \langle k \rangle - 1 = -0.45$ . After reconstruction  $Q_M = 0.04$  is classical and close to the expected, zero value. In Fig. 3 (b) we present Mandel  $Q$  parameters and fidelity of reconstruction  $\mathcal{F} > 0.99$  for test states of different mean values  $\langle n \rangle$ . Note that  $Q_F$  is always negative, even for illumination level of 0.05 photons per single photon detector area.

Further insights into the operation of our method can be gained from the reconstruction of joint statistics, where artificial sub-shot-noise correlation can easily occur without proper reconstruction procedures. As a test state we used equiprobable switched pairs of coherent states simultaneously illuminating two tiles, labeled  $i = 1, 2$ . The mean number of photons  $\langle n_i \rangle$  at the  $i$ -th tile was switched between  $\bar{n}_i$  and  $\bar{n}'_i$ . The resulting state

has non-trivial joint statistics exhibiting classical correlations of photon numbers between subsystems. Its Fano noise reduction factor is  $R = 1$  and Mandel parameters of marginal statistics are  $Q_M > 0$  for  $\bar{n}_i \neq \bar{n}'_i$ . We post-selected two similar but not identical tiles which were calibrated together in QDT process yielding the equivalent number of on-off detectors  $N^{(1)} = 4.9$  and  $N^{(2)} = 6.3$  and conditional probabilities  $\Pi_{k_1|n_1}^{(1)}$  and  $\Pi_{k_2|n_2}^{(2)}$  respectively. We checked there was no crosstalk between the tiles. We present a typical reconstruction result in Fig. 4 with high fidelity  $\mathcal{F} = 0.992$ . Note we succeeded in fixing artificial sub-poissonian correlation measured in photo-event count from  $R = 0.71$  to  $R = 1.01$  value after reconstruction. In Fig. 5 we plot measured and the reconstructed Mandel parameters  $Q_M$  and  $Q_F$  and the Fano noise reduction factor for a variety of test states of the above type for fixed number of photoelectrons  $\bar{n}_1 = 4.4$  as a function of  $\bar{n}'_1$ . Note for each test state the Fano factor for photo-events was always artificially non-classical and fixed by the reconstruction.

For  $\bar{n}'_1 < 1.5$  we observe the particularly interesting situation in which the directly measured marginal statistics are superpoissonian ( $Q_F > 0$ ) and the joint statistic is subpoissonian ( $R < 1$ ). Note that this mimics the two mode squeezed state or their mixture. In both cases the marginal statistics are superpoissonian thermal or multimode thermal. Without the reconstruction procedure the correlated classical state which we used is easily mistaken with its quantum counterpart.

Both the single mode statistics and the two mode joint statistics were reliably reconstructed up to the light intensity level corresponding to one photon per single photon detection area  $\langle n_i \rangle = (\bar{n}_i + \bar{n}'_i)/2 \simeq N^{(i)}$ . In this intensity regime we were able to remove artificial non-classical effects from the reconstructed statistics and the fidelity of reconstruction consistently exceeded  $\mathcal{F} > 0.99$ .

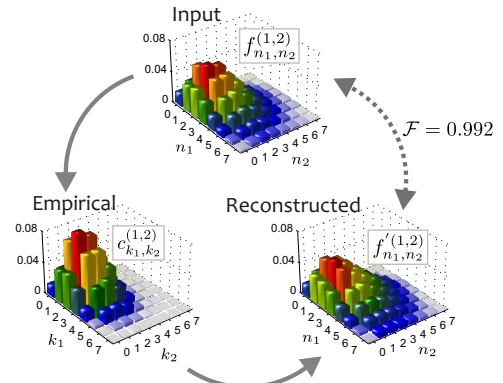


Figure 4. Histograms of joint statistics related to pair of tiles. The input state  $f_{n_1, n_2}^{(1,2)}$ , raw measured data  $c_{k_1, k_2}^{(1,2)}$  and reconstructed state  $f'_{n_1, n_2}^{(1,2)}$  with high fidelity  $\mathcal{F}$ . Two calibrated tiles with  $N^{(1)} = 4.9$  and  $N^{(2)} = 6.3$  were illuminated by equiprobably alternated statistical mixture of coherent states, with  $\bar{n}_1 = 2$ ,  $\bar{n}'_1 = 3.7$ .

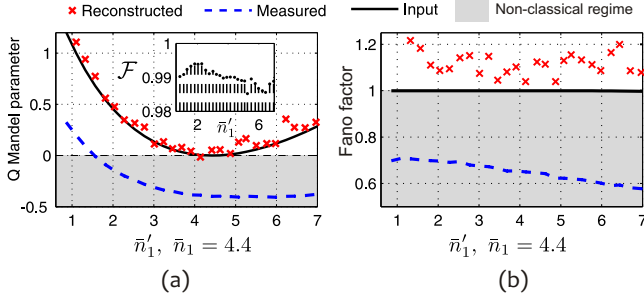


Figure 5. Results of joints statistics reconstruction of equiprobably alternated statistical mixtures of coherent states. (a) Mandel parameters for photo-events  $Q_F$  are superpoissonian for  $\bar{n}'_1 < 1.5$ . (b) Noise reduction Fano factor for photo-events is always non-classical. Reconstructed values consistently remain classical and are close to the expected values.

These observations set the limit of useful operation of our method up to one photon per single photo-event detection area on average. It is two orders of magnitude higher than recently reported values [10, 16]. This enhancement is enabled by proper one-time quantum detector tomography and proper numerical state reconstruction. The higher permissible light intensity means increased maximum photon number resolving capability or, by dense tiles subdivision, increased spatial resolution of the imaging system. For instance our particular system can be used as an array of 10000 tiles capable of detecting up to 6 photons on average, each at a frame rate of 200 Hz. The dark count rate equals  $6 \cdot 10^{-6}$  per each 100 ns gate duration per tile and can be further reduced by two orders of magnitude by cooling a photocathode.

In conclusion, we devised and demonstrated a novel method for measuring multiphoton statistics with spatial resolution using intensified sCMOS detector. Our method allowed in the high-illumination regime to retrieve input photon statistics with high fidelity  $\mathcal{F} > 0.99$ , free from corruptible saturation effects. We verified the method using one and two mode classical states consistently yielding classical values of Mandel and Fano parameters for one and two dimensional statistics respectively. The method consists in one-time calibration with appropriate quantum detector tomography (QDT) yielding conditional probabilities determining the operation of the camera tiles. Data processing in our method is universal owing to application of QDT techniques, avoiding altogether the need to develop analytical hardware description [14] which is apparatus-specific and may often become overly complex. We established the applicable limit of operation of the method to the average illumination level of one photon per single photon detection area far beyond the current limitations [10, 16]. Our results pave the way to efficient and faithful imaging of multiphoton quantum states of light.

We acknowledge R. Demkowicz-Dobrzański, C.

Radzewicz and J. Iwaszkiewicz. Project was financed by the National Science Centre no. DEC-2013/09/N/ST2/02229, DEC-2011/03/D/ST2/01941, Polish NCBiR under the ERA-NET CHIST-ERA project QUASAR.

## References

1. S. Walborn, D. Lemelle, M. Almeida, and P. Ribeiro, Phys. Rev. Lett. **96**, 090501 (2006). (document)
2. D. S. Tasca, R. M. Gomes, F. Toscano, P. H. Souto Ribeiro, and S. P. Walborn, Phys. Rev. A **83**, 052325 (2011). (document)
3. R. H. Hadfield, Nature Photon. **3**, 696 (2009). (document)
4. M. D. Eisaman, J. Fan, A. Migdall, and S. V. Polyakov, Rev. Sci. Instrum. **82**, 071101 (2011). (document)
5. K. Yu Spasibko, F. Toppel, T. Sh Iskhakov, M. Stobińska, M. V. Chekhova, G. Leuchs, New J. Phys. **16**, 013025 (2014). (document)
6. J. Rehacek, Z. Hradil, O. Haderka, J. Perina, and M. Hamar, Phys. Rev. A **67**, 061801 (2003). (document)
7. D. Achilles, C. Silberhorn, C. Sliwa, K. Banaszek, I. A. Walmsley, M. J. Fitch, B. C. Jacobs, T. B. Pittman, and J. D. Franson, J. Mod. Optic. **51**, 1499 (2004). (document)
8. I. Afek, A. Natan, O. Ambar, and Y. Silberberg, Phys. Rev. A **79**, 043830 (2009). (document)
9. T. Gerrits, B. Calkins, N. Tomlin, A. E. Lita, A. Migdall, R. Mirin, and S. W. Nam, Opt. Express **20**, 23798 (2012). (document)
10. M. P. Edgar, D. S. Tasca, F. Izdebski, R. E. Warburton, J. Leach, M. Agnew, G. S. Buller, R. W. Boyd, and M. J. Padgett, Nat. Commun. **3**, 984 (2012). (document)
11. R. Fickler, M. Krenn, R. Lapkiewicz, S. Ramelow, and A. Zeilinger, Sci. Rep. **3**, 1914 (2013). (document)
12. R. S. Aspden, D. S. Tasca, R. W. Boyd, and M. J. Padgett, New J. Phys. **15**, 073032 (2013). (document)
13. G. Brida, M. Genovese, and I. Ruo Berchera, Nature Photon. **4**, 227 (2010). (document)
14. O. Haderka, J. Perina, and M. Hamar, Phys. Rev. A **71**, 4 (2005). (document)
15. J.-L. Blanchet, F. Devaux, L. Furfaro, and E. Lantz, Phys. Rev. Lett. **101**, 233604 (2008). (document)
16. D. S. Tasca, M. P. Edgar, F. Izdebski, G. S. Buller, and M. J. Padgett, Phys. Rev. A **88**, 013816 (2013). (document)
17. R. Machulka, O. Haderka, J. Perina, M. Lamperti, A. Allevi, and M. Bondani, arXiv:1405.1190, (2014). (document)
18. J. S. Lundeen, A. Feito, H. Coldenstrodt-Ronge, K. L. Pagnell, C. Silberhorn, T. C. Ralph, J. Eisert, M. B. Plenio, and I. A. Walmsley, Nature Phys. **5**, 27 (2008). (document), 2
19. a. Feito, J. S. Lundeen, H. Coldenstrodt-Ronge, J. Eisert, M. B. Plenio, and I. a. Walmsley, New J. Phys. **11**, 093038 (2009). (document), 2
20. T. J. Bartley, G. Donati, X.-M. Jin, A. Datta, M. Barbieri, and I. A. Walmsley, Phys. Rev. Lett. **110**, 173602 (2013). (document)
21. J. Sperling, W. Vogel, and G. S. Agarwal, Phys. Rev. A **85**, 023820 (2012). (document)